Polymer Bulletin 58, 65–74 (2007)
DOI 10.1007/s00289-006-0635-y

Polymer Bulletin

Poly(imide-amide)-poly(ethylene glycol) hybrid networks: nanostructure, molecular dynamics and membrane properties

Vladimir A. Bershtein[1] (✉), Larisa M. Egorova[1], Pavel N. Yakushev[1], Vladimir Sindelar[2], Petr Sysel[2], Tatiana E. Sukhanova[3], Irina P. Dobrovolskaya[3], Anatoly I. Grigoriev[3], Sotiria Kripotou[4], Polycarpos Pissis[4]

[1]Materials Dynamics Laboratory, Ioffe Physico-Technical Institute of Russian Academy of Sciences, 194021 St. Petersburg, Russia
[2]Department of Polymers, Institute of Chemical Technology, 16628 Prague 6, Czech Republic
[3]Polymer Morphology Laboratory, Institute of Macromolecular Compounds of Russian Academy of Sciences, 31, Bolshoi pr. V.O., 199004 St. Petersburg, Russia
[4]Department of Physics, National Technical University of Athens, 15780 Athens, Greece
E-mail: vbersht@polmater.ioffe.ru

Received: 15 July 2005 / Revised version: 19 December 2005 / Accepted: 14 January 2006
Published online: 27 July 2006 –

Summary

Nanometer-scale structure, molecular dynamics (at 100-580 K) and membrane properties were studied in two series of poly(imide-amide) (PIA)-poly(ethylene glycol) (PEG) hybrid networks with regularly varied composition and different lengths of PEG crosslinks (M_n = 1 000 or 3 400). Combined WAXD/SAXS/polarized microscopy/DSC/DRS/TSDC/creep rate spectroscopy (CRS) analysis of these hybrids was performed. Depending on their composition, semicrystalline or mesomorphous, or amorphous state, and nanostructural heterogeneity were observed for these networks. They could be subdivided into (a) the PIA-rich hybrids with spatially isolated PEG domains, "suppressed" dynamics in the PEG glass transition, and PIA domains with T_g = 520-570 K (group 1), and (b) the other hybrids with a continuous PEG phase and low-temperature glass transition only (group 2). Heterogeneity in segmental dynamics was revealed by CRS over the temperature range from T_g^{PEG} to T_g^{PIA}. In the second group of hybrids, the permeability coefficients were higher, by two or three orders of magnitude, for organic vapors than those for air gases.

Introduction

In recent years, steadily increasing attention has been paid to hybrid polymer networks consisting typically of covalently bound rigid and relatively "soft" flexible-chain components. Such hybridization is aimed at modifying properties of the basic polymer or combining, to some extent, the merits of both constituents within one material.

Presented at 44th P.M.M. Microsymposium "Polymer Gels and Networks", Prague, 10–14 July 2005

Thus, high-performance membranes for separation of organic vapors from air gases were obtained from the poly(imide-amide)-poly(ethylene adipate) hybrid networks [1,2]. Silica nanoclusters, chemically incorporated into polyimide (PI), modified dynamics in PI and resulted in increasing thermal lifetime of the PI-silica hybrids as compared with neat PI [3]. Plurality of glass transitions in polycyanurate-poly(tetramethylene glycol) hybrid networks [4] provided a substantial rise in their tensile strength as compared with that for brittle polycyanurate network [5].
The present article describes the peculiarities of nanostructure, dynamics and membrane properties in poly(imide-amide)-poly(ethylene glycol) (PIA-PEG) hybrid networks. It was assumed that these hybrids could combine high permeability of elastomer membranes with high thermal and mechanical resistance of PI.

Experimental

Materials

PIA-PEG hybrid networks were synthesized in accordance with the procedures described in detail elsewhere for similar [6] and PIA-PEA networks [1,2]. The "intermediate" products in the synthesis were (a) poly(amic acid) based on pyromellitic dianhydride (Chriskev, USA) and 4,4′-oxydianiline (Aldrich, Czech Republic), [PAA(PMDA-ODA)], and (b) 4-methyl-1,3-phenylene diisocyanate (TDI)-terminated poly(ethylene glycol), where the isocyanate groups were end-capped with phenol [Ph-TDI-PEG]. The latter permitted to prevent the premature reaction between both components, PAA(PMDA-ODA) and Ph-TDI-PEG, during their mixing. PEG with the number-average molar masses, M_n = 1 000 g/mol (PEG1000) and 3 400 g/mol (PEG3400) (Aldrich), were used in the experiments.
PAA(PMDA-ODA) with uncontrolled molecular weight was prepared by the reaction of equimolar amounts of a dianhydride and a diamine in 1-methyl-2-pyrrolidone (NMP, Merck) for 24 h at room temperature; the solid content was 10 wt. %. The PEG terminated with TDI (TDI-PEG) was prepared by the reaction of TDI and PEG (10 wt. % solution in toluene) in a molar ratio of 3:1. The reaction mixture was allowed to react for 2 h at room temperature. Then, phenol was added into the mixture (molar ratio TDI-PEG:PhOH = 1:2) and it was allowed to react for additional 3 h; the product was obtained by precipitation into diethyl ether.
The PIA-PEG hybrid films with a thickness of 20-50 μm and different compositions were prepared from PAA solution in NMP and Ph-TDI-PEG mixed in various ratios. The mixtures were cast onto a glass plate. After evaporating the solvent, the films were subjected to thermal treatment at 70, 100, 150, 200 and 230°C for 10, 1, 1.2 and 1 h, respectively. During the thermal treatment, phenol was released and the deprotected isocyanate groups of TDI-PEG reacted with carboxylic groups of PAA with formation of amide groups. Consequently, two reactions, both PAA imidization and crosslinking (hybridization of both components), proceeded in parallel on heating. As a result, the networks formed were complex in their chemical structures, and contained basically imide but also amide groups in the backbone. The higher crosslinking agent content was introduced into a composition, the higher amount of crosslinks between PI chains and the lower polyimide moiety/polyamide moiety ratio were reached. Along with neat PEG(3400) and PI, two series of the hybrid networks were prepared and studied, with relatively short (PEG1000) and long (PEG3400) crosslinks and PIA/PEG weight ratios of 20/80, 40/60, 50/50, 60/40 and 80/20.

Techniques

Wide-angle X-ray diffraction (WAXD) measurements were performed in transmission mode at room temperature using a DRON-3 (Russia) X-ray diffractometer with CuK_α radiation (λ = 1.54 Å) and Ni-filter. Data were collected for a continuous scan at a rate of 2°C/min over a range of 2θ = 4-35°. The measured X-ray diffraction intensities were corrected for the background and then normalized by matching the integrated intensity over the range of 2θ = 4-45° The interplanar distance d was determined with the accuracy 10%. Small-angle X-ray scattering (SAXS) measurements were performed on a Kratky collimation system equipped with a position-sensitive detector, using Ni-filtered CuK_α radiation. The samples as the film bundles of about 0.5 mm thickness were used. The scanning rate was 2°C/min over a range of angles φ = 3-18 min. The polarized optical microscopy study was performed using microscope equipped with a Boetius heating table.

DSC curves were measured over the temperature range from 150 to 570 K, in nitrogen atmosphere, using a Perkin-Elmer DSC-2 apparatus. Two scannings at the heating rate 20 K/min, with the cooling rate 320 K/min, were performed for each sample. The PEG melting temperature T_m, melting range ΔT_m, degree of crystallinity χ, and glass transition heat capacity steps ΔC_p and temperatures (at the half-height, T_g, the onset, T_g', and completion, T_g'', of a heat capacity step) were determined. The accuracy of T_g, T_m, ΔC_p and χ determination was ± 2 K, ± 1 K, ± 5%, and ± (3-5%), respectively.

Dielectric relaxation spectroscopy (DRS) measurements of the complex dielectric permittivity, $\varepsilon^*=\varepsilon'-i\varepsilon''$, were performed as a function of frequency $f \approx 10^{-2}$-10^5 Hz. A Schlumberger frequency response analyzer (FRA, SI 1260), supplemented with a buffer amplifier of variable gain (Chelsea Dielectric Interface), was used.

The thermally stimulated depolarization current (TSDC) measurements were performed using a laboratory-made apparatus operating over the 77-300 K range. The film sample was inserted between the brass plates of the capacitor and polarized in the electric field E_p= 6 kV/cm at temperature T_p = 300 K for the time period t_p= 5 min. The latter was large in comparison with the relaxation time at T_p of the dielectric dispersion under investigation. With the electric field still applied, the sample was cooled with a rate of 6 K/min to temperature T_0 = 88 K (low enough to prevent depolarization by thermal excitation), and then was short-circuited and heated at the rate 3 K/min. A discharge current was generated as a function of temperature, which was measured with a sensitive electrometer. The equivalent frequency of TSDC measurements spans the range $10^{-4} < f < 10^{-2}$ Hz [7].

Laser-interferometric creep rate spectroscopy (CRS) was used for discrete analysis of segmental dynamics over the temperature range from –80 to ~300°C. This method, developed at the Ioffe Institute, the schemes of the CRS setups, and the experimental technique have been described in detail elsewhere [8-11]. CRS consists in precise measuring low creep rates at constant small stress, much lower than the yield stress, as a function of temperature (creep rate spectrum). A laser interferometer based on the Doppler effect is used for this purpose. The tensile stress 5 MPa was chosen in this work as capable of inducing sufficient creep rates to be measured while maintaining a good spectral resolution. The time from the moment of loading to the onset of measurement was kept constant (t=10 s) in measuring a creep rate spectrum. Normally, a sample was cooled to the lowest temperature of the range under study, and the stress was applied for 1 min to get the interferogram. Then, the sample was unloaded, heated at the rate 1 K/min to a temperature by 5 K higher, and loaded again,

and so on. CRS allowed to measure creep rates on the basis of deformation increment of ca. 0.01-1.0% and manifested superiority in resolution and sensitivity to widespread relaxation spectrometry techniques. Satisfactory reproducibility of the CR spectra may be seen, e.g., from Fig. 7 in Ref. [12]. The correlative frequency of the CRS experiments was $\nu_{corr}=(2\pi t)^{-1}\approx 10^{-2}$ Hz, i.e. the time conditions were close to those in the DSC experiments.
The differential permeation method, using the laboratory-made instrument [1], was utilized to determine the permeability coefficients *P* of films at 20°C and 1 atm.

Results and discussion

Structure

High crystallinity was observed by WAXD for neat PEG (3400) films where intense reflections, corresponding to interplanar distances *d* = 4.6, 3.9, 3.5, 2.5, 2.3 Å, and broad peak (amorphous halo) with *d* = 10.0 Å were observed (not shown here).
Figure 1 shows transmission WAXD diffractograms for a few PIA-PEG hybrid networks. One can see that crystallinity of the hybrids with PEG (3400) decreases with increasing PIA content. For the 20PIA-80PEG (3400) network, the same reflections as for neat PEG (3400) were observed but the intensity of the most pronounced reflections with *d* = 4.6 and 3.9 Å decreased. For the 40PIA-60PEG (3400) network, besides decreasing the narrow reflections, amorphous halo with *d* = 4.3 Å arose. Only two broad peaks with spacings *d* = 11.0 and 4.5 Å. were observed for the 50PIA-50PEG (3400) hybrid, and polarized microscopy indicated that this sample is a mixture of amorphous and mesomorphous domains. For the 60PIA-40PEG (3400) and 80PIA-20PEG (3400) films, the mesomorphous structure was shown since two broad reflections with spacings *d* = 16.0 and 4.5 Å were observed, and polarized microscopy showed a bright anisotropic "picture" for these hybrids. WAXD diffractograms of the hybrids with PEG (1000) indicated their amorphous structure. Thus, the broad reflections with *d* = 11.0 and 4.5 Å, or 16.0 and 4.5 Å were observed in the diffractograms of the 20PIA-80PEG (1000) and 50PIA-50PEG (1000) networks, respectively (Fig. 1).

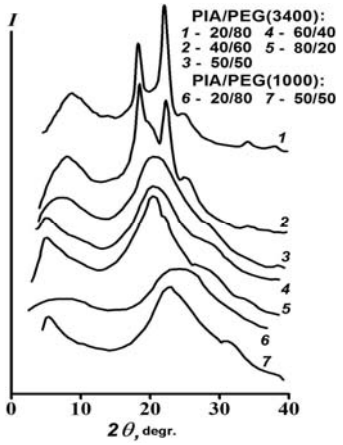

Figure 1. Transmission WAXD diffractograms of the PIA-PEG hybrid networks.

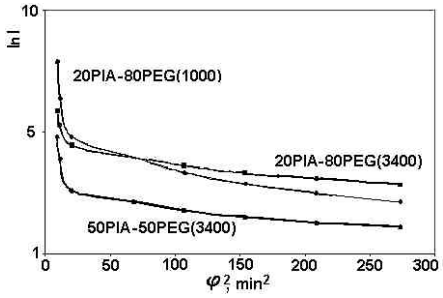

Figure 2. SAXS intensity (ln *I*) versus square of scattering angle φ plots (Guinier co-ordinates) for three hybrid networks.

Figure 2 shows the SAXS intensity versus φ^2 plots obtained for three hybrid networks. These dependences indicate density nanoheterogeneity in the hybrids, and some difference in scattering ability.
The latter decreased in the order: 20PIA-80PEG (1000) – 20PIA-80PEG (3400) – 50PIA-50PEG (3400) hybrids. The curves show the bend at $\varphi \approx 6$ min that indicates the presence of scattering domains with two sizes. Radius of gyration R_g was calculated from scattering curves; two values, R_{g1} = 70 nm and R_{g2} = 11 nm, were estimated. It was also shown that the 50PIA-50PEG (1000) network was the most nanohomogeneous since its SAXS was practically commensurable with background.

Dynamics

DSC curves were obtained over the range 150-570 K covering the regions of PEG glass transition and melting, and PIA/PI glass transition.

Figure 3 shows the curves obtained at low temperatures on heating the PIA-PEG networks, with the longer and shorter PEG crosslinks, cooled from 290 to 150 K with the rate 320 K/min. One can see the PEG glass transition within the range of 210-270 K and slightly higher T_g^{PEG} values for shorter crosslinks, due to the enhanced constraining influence of the rigid phase on their dynamics. Different PEG glass transition behavior is observed for two groups of the hybrids. For the PIA-rich networks with 20 wt. % PEG or 40 wt. % PEG(1000) (group 1), practically total suppression of segmental dynamics in the PEG glass transition by PIA chains is observed whereas, for the other compositions (group 2), a pronounced transition may be seen.
Melting peaks at ~ 300-330 K (not shown here) were also observed in the DSC curves, in the first scanning, for partly-crystalline samples having longer PEG crosslinks. Figure 4 shows the characteristics of PEG melting and glass transitions as a function of hybrid composition. These plots illustrate, in accordance with the above WAXD data, reduction of the PEG crystallinity degree with increasing PIA content and total amorphization of the PEG (3400) component at the PIA content over 50 wt. % in the hybrids, as well as amorphous state of PEG(1000)-containing networks. Besides, total suppression of PEG (1000) glass transition at 60-80% PIA in the hybrids was shown ($\Delta C_p^{PEG} \rightarrow 0$). On the other hand, the slight glass transition at 550-570 K, indicating the presence of PIA or PI nanodomains, could be discerned in the first scanning for the hybrids with 20-40 wt. % PEG (1000) (not shown here).

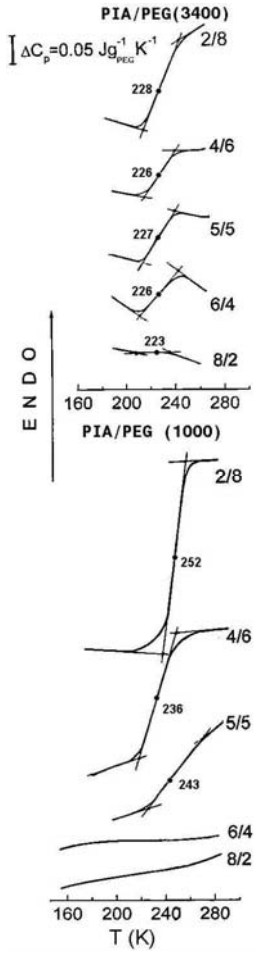

Figure 3. DSC curves of PIA-PEG networks with indicated PIA/PEG weight ratios obtained in the temperature region of PEG glass transition. Heating rate v = 20 K/min.

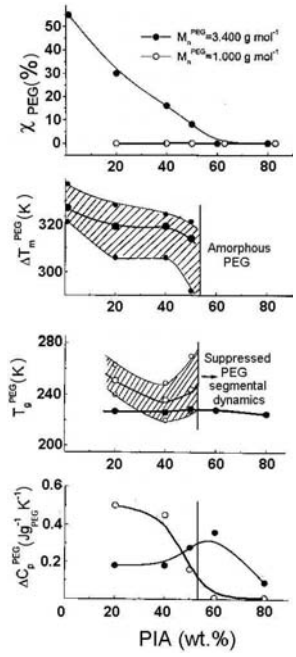

Figure 4. PIA-PEG networks: crystallinity degree χ, melting range ΔT_m, glass transition temperatures (T_g', T_g, T_g''), and heat capacity step ΔC_p in the glass transition, for PEG component only, as a function of the PIA content in a hybrid network.

DRS measurements, performed at 20°C over the broad frequency range, allowed to conclude on morphology of the hybrids. These results confirmed that the samples under study could be classified into two groups: group 1 of PI-rich samples (the hybrids with 20 wt. % PEG or 40 wt. % PEG (1000), and group 2 of the other samples. Figure 5 shows that no conductivity effects in the $\varepsilon'(f)$ dependences, and no tendency to manifesting a plateau at low frequencies in the $\sigma_{ac}(f)$ plots are observed for the samples of group 1 and for neat PI. On the contrary, for the hybrids of group 2, conductivity effects in the $\varepsilon'(f)$ plots are rather strong and increase with increasing PEG content and chain length. These results suggest that PEG forms a continuous phase in the hybrids of group 2 but spatially isolated, discrete PEG domains in the samples of group 1.

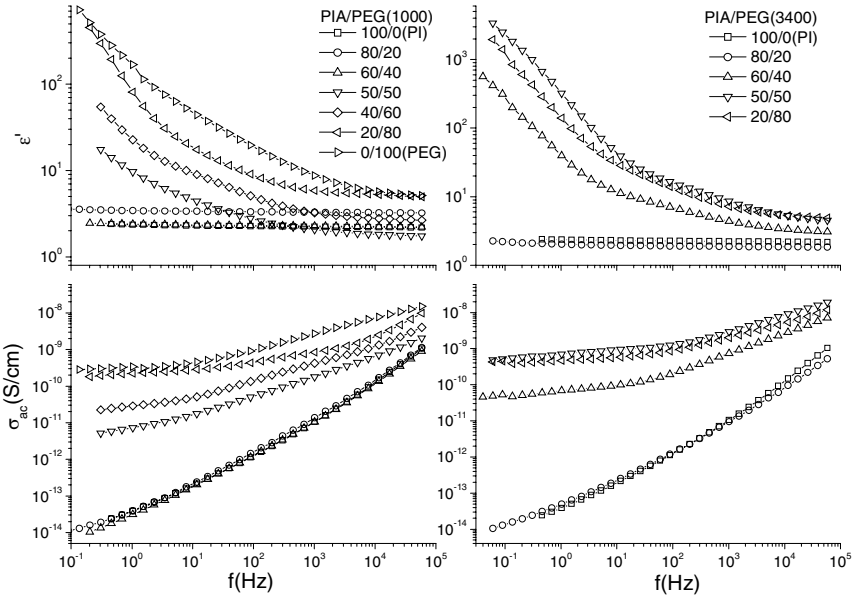

Figure 5. Real part of dielectric permittivity ε' and ac conductivity σ_{ac} at 298 K versus frequency for the indicated PIA-PEG networks and neat PI and PEG.

Figure 6 shows that the TSDC thermograms for the PIA-PEG (1000) hybrids demonstrate three peaks. The γ -peak, corresponding to torsional vibration of the imide ring [13], is located at 145 K for PI but slightly shifted to higher temperatures in the hybrids. The hybridization effect resulted also in a considerable rise of this peak with PEG content, obviously due to loosened packing of PIA chains and increase in free volume.

Again, as in DSC experiments, the PEG glass transition (α) peak is located in the TSDC plots at ~250 K for the hybrids of group 2 but is suppressed for the hybrids of group 1. In the latter case, only a small peak was observed, by an order of magnitude lower, at 270-280 K, which may be also associated with a conductivity effect.

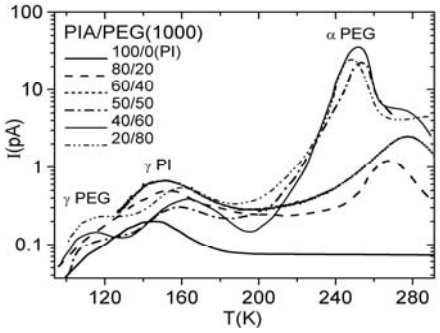

Figure 6. TSDC thermograms obtained for the indicated PIA-PEG networks and PI.

The CR spectra, obtained under tensile stress of 5 MPa at 170-580 K, provided more detailed information on segmental dynamics in PIA-PEG networks, and allowed to estimate their creep resistance at elevated temperatures. Additionally, the discrete CR spectra revealed a pronounced dynamic heterogeneity over the broad temperature range, from T_g^{PEG} to T_g^{PI} (Fig. 7).

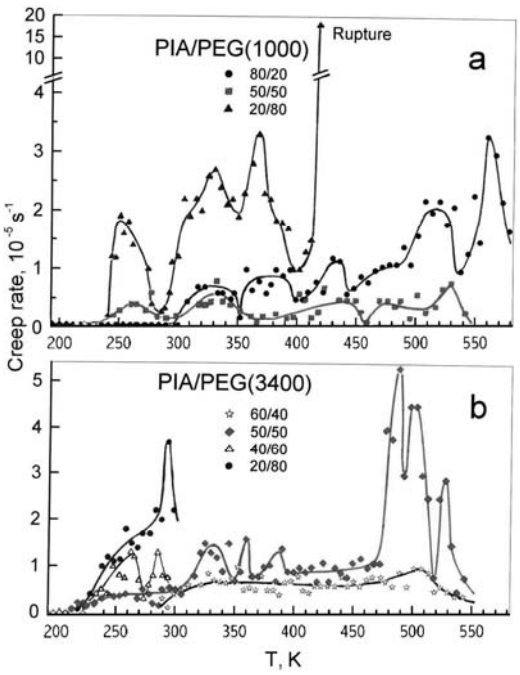

Figure 7. Creep rate spectra obtained under tensile stress of 5 MPa and t = 10 s for the PIA-PEG hybrid networks with (a) the shorter (M_n=1 000 g/mol) and (b) the longer (M_n=3.400 g/mol) PEG crosslinks. The PIA/PEG weight ratios in the hybrids are indicated.

The complex CR spectral contours consist of a few partly overlapping peaks. The peak heights strongly vary with hybrid composition. The peak at the lowest temperatures 220-270 K, must be assigned to "usual" glass transition in PEG crosslinks. Its intensity decreases with the PIA content in a hybrid; the peak is totally suppressed for the 80PIA-20PEG composition. Simultaneously, for this hybrid T_g^{PI}, a peak at ~560 K, i.e., PI nanodomains can be observed.

The CR peak at around 300 K in the spectra of networks with 60 or 80 wt. % PEG (3400) may be presumably related to melting of PEG(3400) crystallites. CR peaks at ~320 and 370 K may, obviously, be associated with PEG segmental motions constrained by rigid PIA chains. This effect of "constrained dynamics", which has been observed also in the PIA-PEA hybrid networks [2], must increase with reduction in the distance between a moving PEG segment and PIA chains. Low creep resistance at $T > 400$ K is observed for 20PIA-80PEG composition (Fig. 7a).

A few peaks in the high-temperature part of the CR spectra, in the region 420-520 K, are associated with the onset of "unfreezing" segmental mobility in PIA chains. Their different temperature location may be treated in the framework of variability in PIA

chain rigidity and T_g^{PIA} plurality. Really, the more crosslinking agent was introduced into a composition, the more amide groups in PIA chains were formed [2,6], and the lower PIA creep resistance is observed. Besides, uneven distribution of amide groups in PIA chains and different cooperativity degree of segmental motion may result in some distribution of T_g^{PIA} values. It should be noted that creep resistance of the hybrids studied at high temperatures depended not only on hybrid composition but also on its nanostructure. Thus, the nanohomogeneous 50PIA-50PEG (1000) hybrid exhibited higher creep resistance than the 80PIA-20PEG (1000) hybrid (Fig. 7a).

Permeability

Table 1. Permeability coefficients for organic vapors and air gas in the PIA-PEG networks

PIA/PEG wt. ratio	M_n^{PEG} [g mol^{-1}]	Permeability coefficient 10^{16} P [mol Pa^{-1}m^{-1}s^{-1}]	
		CO_2	methanol
80/20	1 000	5.80	non-measurable
60/40	1 000	12.34	156
50/50	1 000	15.10	6282
40/60	1 000	25.30	15897
20/80	1 000	44.60	50909
80/20	3 400	30.79	604
60/40	3 400	37.00	15487
50/50	3 400	93.70	20694
40/60	3 400	117.80	62375
20/80	3 400	101.25	68800

Table 1 shows the permeability coefficients P for CO_2 and methanol in the networks studied. One can see that the P values are strongly dependent on network composition; besides, the permeability is higher in the case of longer crosslinks. Low permeability (not far from that of neat PIA) is observed for the PIA-rich networks of group 1, i. e., for 80PIA-20PEG (1000), 60PIA-40PEG (1000) and 80PIA-20PEG (3400) hybrids which are characterized by spatially isolated PEG domains with suppressed glass transition dynamics (see above). In contrast, with increasing PEG content in the networks, a slight rise in $P(CO_2)$ value but a sharp increase in $P(CH_3OH)$ values, by a few orders of magnitude, were observed. As a result, high selectivity $\alpha = P(CH_3OH)/P(CO_2) \approx$ 400-1000 was reached for the hybrids of group 2 where PEG formed a continuous phase. Thus, the latter was characteristic of the films with 40 wt. % of PEG (3400) exhibiting also good mechanical resistance at elevated temperatures (Fig. 7b). High α values at 20°C were associated with "unfreezing" segmental dynamics in the PEG glass transition which provided increased diffusion ability of films. A comparison of Table 1 and Figs. 3-7 shows a direct connection between PEG crosslink dynamics and membrane properties of the PIA-PEG hybrids.

Conclusions

1. Combined study, using seven complementary techniques, showed quite different nanostructural state, dynamics and thermal/mechanical stability in PIA-PEG hybrid networks, depending on their composition and PEG crosslink length.

2. The networks with short crosslinks were amorphous, whereas the structure of the networks with longer ones gradually changed with increasing PIA content, from semicrystalline to mesomorphous/amorphous. Nanostructural heterogeneity, with two prevailing sizes of scattering domains, R_{g1}≈10 nm and R_{g2}≈700 nm, was observed for the hybrids.
3. Reciprocally sustaining DSC/DRS/TSDC/CRS data formed a reliable idea of the dynamics and morphology in the PIA-PEG networks. Two kinds of hybrids were identified in these experiments. For PIA-rich hybrids, "suppressed" glass transition dynamics in spatially isolated PEG domains, and distinct PIA/PI domains with T_g = 550-570 K were observed. The other hybrids manifested only low-temperature PEG glass transition in the DSC curves, and were characterized by a continuous PEG phase resulting in a strong conductivity effect. CRS data showed that hybridization resulted in large heterogeneity in segmental dynamics over the (T_g^{PEG} - T_g^{PI}) temperature range, due to constraining PEG dynamics and PI/PA unit distribution.
4. The membrane properties of the hybrids are in accordance with the dynamics in PEG crosslinks. Some of PIA-PEG hybrids combined high permeability to organic vapors and good permselectivity with improved thermal and mechanical resistance. The 50PIA-50PEG (1000) and 60PIA-40PEG (3400) compositions are high-performance, effective membranes for separation of hot solvent/air streams.

References

1. Sindelar V, Sysel P, Hynek V, Friess K, Sipek M, Castaneda N (2001) Collect Czech Chem Commun 66:533
2. Bershtein VA, David L, Egorov VM, Egorova LM, Yakushev PN, Pissis P, Sysel P, Sindelar V (2002) Polymer 43:6943
3. Bershtein VA, Egorova LM, Yakushev PN, Georgoussis G, Kyritsis A, Pissis P, Sysel P, Brozova L (2002) J Polym Sci, Part B: Polym Phys 40:1056
4. Bershtein VA, David L, Egorov VM, Fainleib AM, Grigoryeva OP, Bey I, Yakushev PN. (2005) J Polym Sci, Part B: Polym Phys 43:3261
5. Fainleib AM, Hourston DJ, Grigoryeva OP, Shantalii TA, Sergeeva LM (2001) Polymer 42:8361
6. Sysel P, Sindelar V, Hobzova R, Nejedla S, Frycova M (2003) Plast Kauc 40:292
7. Van Turnout J Thermally Stimulated Discharge of Electrets, in Sessler GM (Ed) Topics in Applied Physics 33 Springer Berlin (1980) 81
8. Peschanskaya NN, Yakushev PN, Sinani AB, Bershtein VA (1994) Thermochim Acta 238:429
9. Peschanskaya NN, Yakushev PN, Sinani AB, Bershtein VA (1997) Macromol Symp 119:79
10. Bershtein VA, Yakushev PN, Karabanova L, Sergeeva L, Pissis P (1999) J Polym Sci, Part B: Polym Phys 37:429
11. Bershtein VA, Yakushev PN, Peschanskaya NN (1999) Macromol Symp 147:73
12. Bershtein VA, Egorova LM, Egorov VM, Peschanskaya NN, Yakushev PN, Keating MY, Flexman EA, Kassal RJ, Schodt KP (2002) J Macromol Sci-Phys 41:797
13. McCrum NG, Read BE, Williams B Anelastic and Dielectric Effects in Polymeric Solids, Wiley New York (1967)